Journal of Crystal Growth 311 (2009) 504–507

Contents lists available at ScienceDirect

Journal of Crystal Growth

journal homepage: www.elsevier.com/locate/jcrysgro

Mass production and characterization of free-standing ZnO nanotripods by thermal chemical vapor deposition

Min-Yeol Choi [a], Hyun-Kyu Park [a], Mi-Jin Jin [a], Dae Ho Yoon [b], Sang-Woo Kim [a,c,*]

[a] School of Advanced Materials and System Engineering, Kumoh National Institute of Technology, Gumi, Gyeongbuk 730-701, Republic of Korea
[b] Department of Advanced Materials Engineering and SAINT, Sungkyunkwan University, Suwon, Gyeonggi 440-746, Republic of Korea
[c] Gumi Materials and Components Technology Supporting Center, Kumoh National Institute of Technology, Gumi, Gyeongbuk 730-853, Republic of Korea

ARTICLE INFO

Available online 24 September 2008

PACS:
71.55.Gs
61.46.Hk
61.72.Mm
78.55.Et
73.63.−b

Keywords:
A3. Chemical vapor deposition processes
B1. Nanomaterials
B2. Semiconducting II–VI materials

ABSTRACT

Mass-productive free-standing ZnO nanotripods were obtained by thermal chemical vapor deposition without introduction of catalysts and substrates. Three arms of ZnO nanotripods had lengths ranging from 300 nm to 1.0 μm and a single-crystalline hexagonal structure. It was found that an inverted triangle-shaped zinc blende ZnO core is located at the center of the grown ZnO nanotripod and a twin structure exists at the interface between each arm. The three arms with extremely narrow diameters below 20 nm were grown along to the [0 0 0 1] *c*-axis and the twin boundary was identified as $(0\,1\,\bar{1}\,3)$. ZnO nanotripods exhibited a relatively weak deep-level emission band as well as strong near band-edge emission in the room-temperature photoluminescence measurement, indicating the high optical quality and low defect density of the ZnO nanotripods.

1. Introduction

In recent years, studies on synthesis, characterization, and applications of one-dimensional (1D) ZnO nanostructures such as nanowires, nanorods, nanotubes, nanoneedles, nanoscale multipods and nanobelts [1–3] have been studied extensively, because ZnO nanostructures have been regarded as a promising nanomaterial in a wide range of applications like solar cells, sensors, light-emitting diodes, piezoelectric nanogenerators, field-effect transistors, and transparent electrodes [4–10]. Among them, ZnO multipod nanostructures have attracted much attention recently due to many advantages of free-standing ZnO multipod nanostructures in networked or branched nano-scale device applications. For example, branched nanostructures provide enhanced electron extraction due to their more large surface area compared with 1D nanostructures in inorganic–organic hybrid photovoltaic devices [10]. Moreover, the multipod structure is strongly effective to realize the formation of branched or linear homo/hetero-junctions by self-assembly in successive growth processes, leading to arbitrary branching nanostructure building blocks.

Especially, a number of research works regarding the synthesis and characterization of ZnO nano-scale tetrapod structures were reported because the tetrapod structure is the simplest [11–13], while ZnO tripod nanostructures were rarely investigated. Thus, formation mechanism and characteristics of ZnO tripod nanostructures are not clear. In addition, mass production of ZnO tripod-shaped free-standing ZnO nanostructures in a thermal chemical vapor deposition (CVD) should be realized for highly efficient large-scale device applications because only a small quantity of ZnO nanostructures can be obtained on substrates and the nanostructures grown via a high-temperature CVD process are of much better material properties than them by other wet chemical routes [14–16].

In this work, we report on mass production of free-standing ZnO nanotripods by thermal CVD as well as their structural and optical properties. Our free-standing ZnO nanotripods compared with the ZnO tetrapods are more efficient to realize nano-scale devices because a tripod structure has a two-dimensionally networked morphology which is easy to manipulate an individual nanostructure.

2. Experiments

Synthesis of free-standing ZnO nanotripods was carried out in a horizontal tube furnace that has two separated heating zone systems. The ZnO and graphite powder mixture with a weight

* Corresponding author at: School of Advanced Materials and System Engineering, Kumoh National Institute of Technology, Gumi, Gyeongbuk 730-701, Republic of Korea. Tel.: +82 54 478 7745; fax: +82 54 478 7769.
E-mail address: kimsw@kumoh.ac.kr (S.-W. Kim).

0022-0248/$ - see front matter © 2008 Elsevier B.V. All rights reserved.
doi:10.1016/j.jcrysgro.2008.09.057

ratio 1:1 was used as a source. The mixed powder was put in to an alumina boat, and then alumina boat was placed at the first heating zone in the tube furnace. The first heating zone was heated to 1100 °C. The second heating zone located at downstream of the first heating zone was maintained at 1000 °C in order to control growth temperature of ZnO nanotripods. After the first and second zones were concurrently heated, both zones were kept for 60 min. The furnace was cooled down to room temperature (RT) after the growth. During the growth process, a constant Ar flow (800 sccm) was introduced as a carrier gas and the mixture gas (25 sccm) of Ar and O_2 with a volume ratio of 9:1, respectively, was used as an oxygen source. The Ar and O_2 mixture gas was directly applied to the second heating zone in order to prevent reaction between graphite and oxygen sources near the place of the first heating zone. The as-synthesized products were collected at the inner alumina tube wall after the cooling to RT was finished.

The morphology of as-grown ZnO nanotripods was examined by field-emission scanning electron microscopy (FE-SEM) and bright-field transmission electron microscopy (BF-TEM) measurements. Structural properties of the nanotripods in an atomic scale were investigated by high-resolution transmission electron microscopy (HRTEM) measurements. In order to characterize optical properties of the ZnO nanotripods, we carried out RT photoluminescence (PL) measurements using a 325 nm He–Cd laser.

3. Results and discussion

Fig. 1(a) shows a photographic image of the ZnO product synthesized by using the mixture powder with 0.8 g as a source material. As shown in the Fig. 1(a), the cloudlike semi-transparent product revealing a white color was collected on the tube wall around the second heating zone. Figs. 1(b and c) shows FE-SEM images of the product shown in the Fig. 1(a). The FE-SEM images clearly show that the as-synthesized product is composed of a great number of tripod-shaped nanostructures with uniform distribution. In order to confirm that the as-synthesized product is ZnO, X-ray diffraction (XRD) measurements of the cloudlike product shown in the Fig. 1(a) were carried out (Fig. 2). The XRD data were analyzed using a standard diffractometer with Cu Kα radiation in the $\theta-2\theta$ configuration. The XRD profile of the product totally coincides with the wurzite ZnO crystal structure, indicating the uniform formation of wurzite-structured free-standing ZnO nanotripods.

BF-TEM images in Figs. 3(a and b) show that the synthesized ZnO nanotripods have diameters below 20 nm. It was confirmed that three arms of ZnO nanotripods with uniform distribution are of lengths ranging from 300 nm–1.0 μm. It should be noted that the grown ZnO nanotripods in this work are of extremely narrow diameters below 20 nm which is much smaller than those of the ZnO nanotripods reported in the previous works [17]. The HRTEM image of a single arm among the three arms is shown in Fig. 3(c). The inset shows a corresponding fast Fourier transformation (FFT) pattern, indicating that the single arm was grown along the *c*-axis. The predominant growth along the *c*-axis is because of a high growth rate along the *c*-axis of ZnO. Wurzite ZnO has relatively larger surface energy in (0 0 0 2) plane than other crystallographic planes [18]. Thus, growth rate is faster *c*-axis direction than other growth directions, resulting in the formation of nanotripods with the arm having a preferred *c*-axis orientation.

Fig. 4(a) shows a TEM image revealing the center area of a single ZnO nanotripod. It is clearly shown that the inverted triangle area located at the core of the nanotripod has an atomic array with a different crystalline structure of each arm. It was found that a zinc blende ZnO [0 1 1] diffraction pattern as well as three sets of wurzite [$\bar{2}$ 1 1 0] diffraction patterns was observed in the selected-area electron diffraction pattern (not shown) recorded from the core shown in Fig. 4(a). Previous works have reported the presence of a zinc blende ZnO core in the ZnO tetrapod [1 1 $\bar{1}$ 2]. They suggest that the formation of the tetrapod structure with four wurzite-structured arms is due to a vapor–solid process. The zinc blende ZnO core acts as a seed that wurzite arms grow. Ding et al. [11] asserted that the four Zn-terminated positively charged surface planes of the zinc blende ZnO core can serve as the fast growth fronts to form the wurzite-structured four arms of the tetrapod structure.

Fig. 4(b) shows the HRTEM image of the circular area marked in the Fig. 4(a). The HRTEM image clearly reveals the interface between two arms of the nanotripod. Figs. 4(c and d) are the FFT patterns of "A" and "B" areas in the HRTEM image of the Fig. 4(b), respectively. The interface plane is identified as (0 1 $\bar{1}$ 3), indicating the formation of the twin boundary between each arm grown along the [0 0 0 1] *c*-axis. We assume that the formation of the tripod structure consisting of a zinc blend core and three

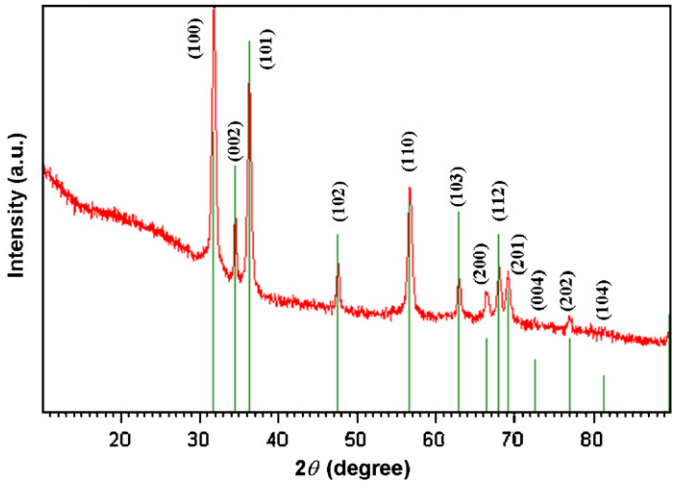

Fig. 2. XRD profile of the cloudlike ZnO product shown in Fig. 1(a).

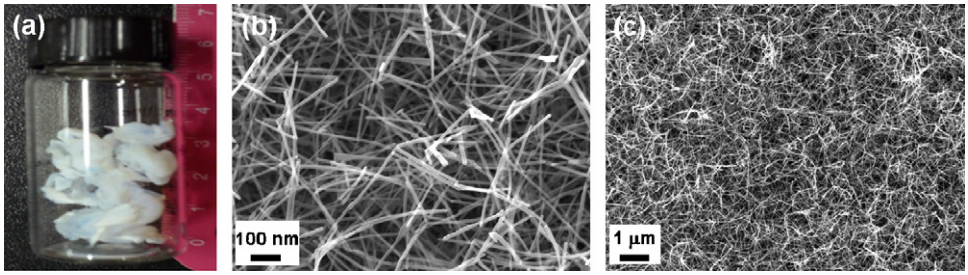

Fig. 1. (a) Photographic image of the ZnO product synthesized by using the mixture powder with 0.8 g as a source material. (b) and (c) show FE-SEM images of the grown ZnO product.

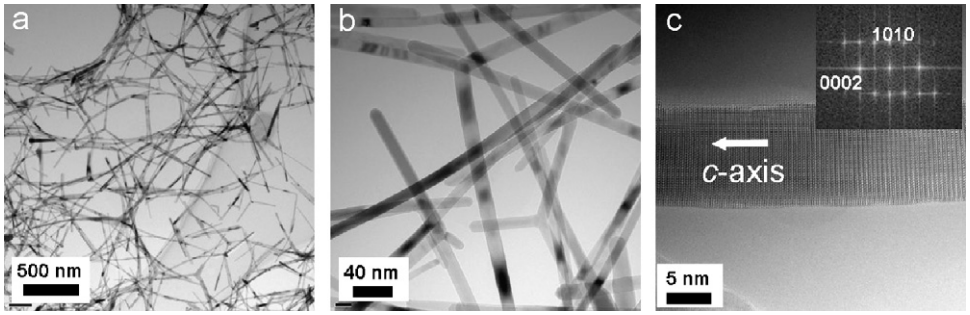

Fig. 3. (a) and (b) show BF-TEM images of the synthesized free-standing ZnO nanotripods. (c) HRTEM image of a single arm among the three arms. The inset is a FFT pattern of the HRTEM image.

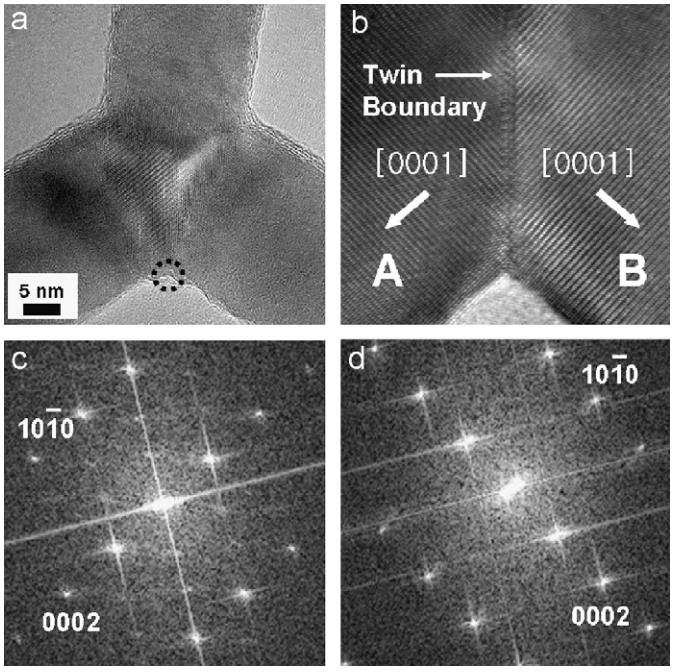

Fig. 4. (a) TEM image revealing the center area of a single ZnO nanotripod. (b) HRTEM image of the circular area marked in Fig. 4(a–d) are FFT patterns of "A" and "B" areas in the HRTEM image of the Fig. 4(b), respectively.

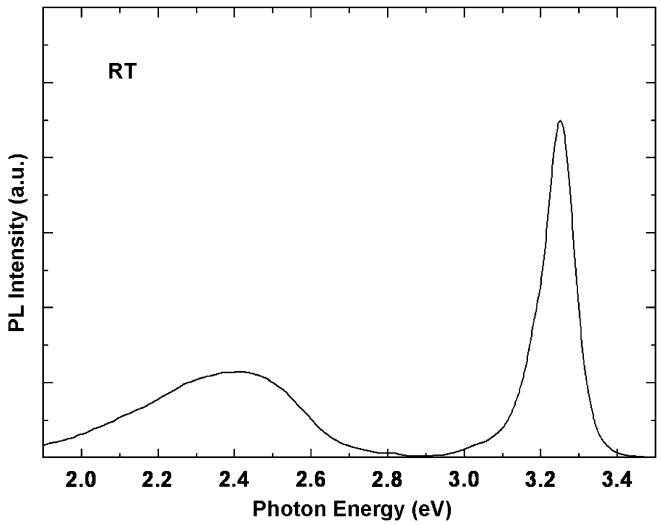

Fig. 5. RT PL spectrum of ZnO nanotripods.

wurzite arms can be explained by the octa-twin model in accordance with the previous report [19]. However, the concrete formation mechanism of the ZnO nanotripods is not clear at the present stage. More detailed crystallographic investigations on the formation mechanism of the ZnO nanotripods should be accomplished.

Here, the growth process of the free-standing ZnO nanotripods in this work is briefly discussed. Firstly, a large number of Zn vapors are generated by heating mixture powder consisting of ZnO and graphite, and then the generated Zn vapors are transported to the second heating zone by the Ar carrier gas. The transported Zn vapor becomes ZnO_x ($x<1$) by the O_2 gas in the Ar and O_2 mixture gas directly introduced to the second heating zone [20]. Secondly, ZnO_x vapors are supersaturated when they pass along the cooler region. Thus ZnO_x vapors are condensed and form ZnO seeds by oxidation of the condensed ZnO_x particles. Finally, after ZnO seed formation, ZnO nanostructures are grown on the ZnO seeds by continuous supply of ZnO_x vapors. In this work, we could know that temperature of the second zone during growth played an important role in the morphology control of ZnO nanostructures. When the second zone temperature was below 1000 °C, irregular hyper-branched ZnO nanostructures were formed in our experiment. On the other hand, a large number of free-standing ZnO nanowires with lengths over 3 μm were obtained at the second zone temperature maintained over 1000 °C. These results will be reported elsewhere in the near future.

Fig. 5 shows a PL spectrum from the nanotripods at RT. The peak around 3.25 eV from the nanotripods is due to near band-edge (NBE) emission. The broad deep-level emission band is located around 2.4 eV. The NBE emission band from the nanotripods prevails while the broad deep-level emission is relatively weak. The deep-level emission in ZnO may be attributed to the singly ionized oxygen vacancy being from the recombination of electrons at the conduction band with holes trapped in oxygen-related defects. Usually, RT PL results of ZnO tetrapods in the previous reports show a broad and strong deep-level emission band as well as weak NBE emission [21–23]. However, strong NBE and relatively weak deep-level emission bands were observed from the ZnO nanotripods in this work as shown in the Fig. 5, suggesting that our ZnO nanotripods have a small number of native point defects and impurities.

4. Conclusions

Mass-productive free-standing ZnO nanotripods were achieved in the thermal CVD process. The grown ZnO nanotripods are of extremely narrow diameter size distributions below 20 nm. It was found that the inverted triangle-shaped zinc blende ZnO core

located at the center of the grown ZnO nanotripod acts as a seed that wurzite ZnO arms grow along to the [0 0 0 1] *c*-axis. In addition, the HRTEM investigation revealed that the twin boundary identified as $(01\bar{1}3)$ exists at the interface between each wurzite ZnO arm. Strong NBE and relatively weak deep-level emission bands were observed from the ZnO nanotripods in the RT PL measurement, indicating that our ZnO nanotripods contain a small number of native point defects and impurities.

Acknowledgements

This work was supported by the Korea Research Foundation Grant funded by the Korean Government (MOEHRD, Basic Research Promotion Fund) (KRF-2007-313-D00475).

References

[1] Z.L. Wang, Mater. Today 7 (2004) 26.
[2] W.I. Park, G.C. Yi, M. Kim, S.J. Pennycook, Adv. Mater. 14 (2002) 1841.
[3] P.X. Gao, C.S. Lao, Y. Ding, Z.L. Wang, Adv. Funct. Mater. 16 (2006) 53.
[4] J.E. Beek, M. Wienk, A.J. Janssen, Adv. Mater. 12 (2004) 16.
[5] Z.L. Wang, J. Song, Science 312 (2006) 242.
[6] J. Goldberger, D.J. Sirbuly, M. Law, P. Yang, J. Phys. Chem. B 109 (2005) 9.
[7] J.K. Sheu, S. Lu, M.L. Lee, W.C. Lai, C.H. Kuo, C.J. Tune, Appl. Phys. Lett. 90 (2007) 263511.
[8] Z. Zhang, L. Sul, Y. Zhao, Z. Liu, D. Liu, L. Cao, B. Zou, s. Xie, Nano Lett. 8 (2008) 652.
[9] Y.Y. Noh, X. Cheng, H. Sirringhaus, J.I. Sohn, M.E. Welland, D.J. Kang, Appl. Phys. Lett. 91 (2007) 043109.
[10] Y.F. Hsu, Y.Y. Xi, C.T. Yip, A.B. Djurisic, W.K. Chan, J. Appl. Phys. 103 (2008) 083114.
[11] Y. Ding, Z.L. Wang, T. Sun, J. Qiu, 90 (2007) 153510.
[12] M.C. Newton, P.A. Warburton, Mater. Today 10 (2007) 50.
[13] F. Wang, Z. Ye, D. Ma, L. Zhu, F. Zhuge, J. Crystal Growth 274 (2005) 447.
[14] K. Yu, Z. Jin, X. Liu, j. Zhao, J. Feng, Appl. Surf. Sci. 253 (2007) 4072.
[15] O. Lupan, L. Chow, G. Chai, B. Roldan, A. Naitabdi, A. Schulte, H. Heinrich, Mater. Sci. Eng. B 145 (2007) 57.
[16] J.W.D. Hsu, D.R. Tallant, R.L. Simpson, N.A. Missert, R.G. Copeland, Appl. Phys. Lett. 88 (2006) 252103.
[17] H. Yan, H. He, J. Pham, P. Yang, Adv. Mater. 15 (2003) 402.
[18] S.W. Kim, Sz. Fujita, H.K. Park, B. Yang, H.K. Kim, D.H. Yoon, J. Crystal Growth 292 (2006) 306.
[19] S. Takeuchi, H. Iwanaga, M. Fujii, Philos. Mag. A 69 (1994) 1125.
[20] Q. Wan, C.L. Lin, X.B. Yu, T.H. Wang, Appl. Phys. Lett. 84 (2004) 124.
[21] C.X. Xu, X.W. Sun, J. Crystal Growth 277 (2005) 330.
[22] Z.G. Chen, A. Ne, F. Li, H. Cong, H.M. Cheng, G.Q. Lu, Chem. Phys. Lett. 434 (2007) 301.
[23] Y. Dai, Y. Zhang, Q.K. Li, C.W. Nan, Chem. Phys. Lett. 358 (2002) 83.